

Indications for a pair-production anomaly from the propagation of VHE gamma-rays

D. Horns^a M. Meyer^a

^aInstitute for Experimental Physics, University of Hamburg, Luruper Chaussee 149, D-22761 Hamburg

E-mail: dieter.horns@physik.uni-hamburg.de

Abstract. In the recent years, the number of detected very high energy (VHE: $E > 100$ GeV) gamma-ray sources has increased rapidly. The sources have been observed at redshifts up to $z = 0.536$ without strong indications for the presence of absorption features in the energy spectra. Absorption is however expected due to pair-production processes of the propagating photons with the photon bath in intergalactic space. Even though this photon density is not well known, lower limits can be firmly set by the resolved emission from galaxy counts. Using this guaranteed background light, we investigate the behaviour of the energy spectra in the transition region from the optically thin to the optically thick regime. Among the sample of 50 energy spectra, 7 spectra cover the the range from optical depth $\tau < 1$ to $\tau > 2$. For these sources, the transition to $\tau > 2$ takes place at widely different energies ranging from 0.4 TeV to 21 TeV. Consistently, in all of these sources, an upturn of the absorption-corrected spectrum is visible at this transition with a combined significance of 4.2 standard deviations. Given the broad range of energies and redshifts covered by the sample, source-intrinsic features are unlikely to explain the observed effect. Systematic effects related to observations have been investigated and found to be not sufficient to account for the observed effect. The pair-production process seems to be suppressed in a similar way as expected in the extension of the standard model by a light (<neV) pseudoscalar (axion-like) particle.

Keywords: gamma ray experiments, axions, absorption and radiation processes

ArXiv ePrint: [1234.5678](https://arxiv.org/abs/1234.5678)

Contents

1	Introduction	1
2	Data analysis and results	2
2.1	Summary of data used	2
2.2	Method to search for the anomaly	4
2.3	Results of the test	5
3	Systematic effects	7
3.1	Systematic effects related to the sources	7
3.2	Energy calibration	9
3.3	End-point of the energy spectra	9
3.4	Mock data set	10
4	Interpretation and discussion	11
4.1	EBL	11
4.2	Implications Pair-production anomaly	11
5	Summary and conclusion	12
A	Energy spectra	18
B	Distribution of averaged residuals	18

1 Introduction

The pair-production process $\gamma + \gamma \rightarrow e^+e^-$ is a well-understood process mostly studied in the laboratory through its inverse process of pair annihilation (e.g. in storage ring experiments). Energetic photons propagating through the intergalactic space undergo pair production with low energy photons of the extragalactic background light (EBL) in the optical (mostly star-light) and infrared (re-emitted light from warm and cold dust) which leads to the attenuation of the primary beam (e.g. [1]) as well as to the formation of an inverse-Compton/pair-production cascade (e.g. [2]). Secondary emission from these cascades may even dominate the observed emission (see e.g. [3, 4] for gamma-ray induced cascades and [5–7] for ultra-high energy proton induced cascades)¹.

In the context of propagation of unpolarized energetic photons, a number of processes have been suggested to modify the standard model behaviour: The pair production process could be affected by Lorentz-invariance violation (LIV) processes [11, 12], kinematic mixing with hidden sector photons [13], as well as conversion and re-conversion of photons into axion-like particles (ALPS) [14, 15]. Such effects modify the resulting optical depth (increasing as well as decreasing it) and may even depend on the particular line of sight to the source [16].

¹the observed broad-band gamma-ray variability of distant Blazars as e.g. H1426+428 ($z = 0.129$) [8, 9], 1ES0229+200 ($z = 0.140$) [9], and 1ES1218+304 ($z = 0.184$) [10] indicates however that the bulk of the observed emission is very likely not produced in cascades.

Therefore, careful spectroscopy of gamma-ray sources in the optically thick regime could effectively probe the existence of pair-production anomalies.

The effect of pair-production during propagation should lead to a pronounced softening of the observed spectra from extragalactic sources with increasing optical depth. Remarkably, a systematic softening of the sources with e.g. increasing redshift has not been observed so far [17]. This fact itself is surprising, but may be explained by e.g. reducing the assumed density of absorbing photons or more subtly, observational effects without invoking any anomalies. Conversely, the apparent lack of absorption has been used to constrain the level of extragalactic background light (EBL) by assuming that the intrinsic shape of the source spectrum should not be harder than plausible models suggest. These analyses constrain the maximum level of the EBL consistently to be close to [18–20] and even slightly below (in the mid-infrared) [21] the guaranteed level of the EBL [22]. The observations of the spectra at energies where the optical depth is low (e.g. with Fermi/LAT) or observation of nearby sources provides a check on the assumptions for the source spectra in an unbiased way [21]. So far, attempts to search for deviations from the expected optical depth have mostly relied on the examination of the power law index of the observed gamma-ray spectrum as a function of redshift. The absence of systematic softening has been interpreted as an indication for ALPS-conversion processes [17, 23]. A more sophisticated approach was followed in [24] where the measured spectra of 3C279, 3C 66A, PKS 1222+216, and PG 1553+113 were fit taking the modification of ALPS-related effects into account. In the following, we search for systematic effects in the energy spectra at the expected transition from optically thin to optically thick in the gamma-ray energy spectra.

2 Data analysis and results

2.1 Summary of data used

We have extracted from the literature all available individual measurements of the differential flux (spectral points) from extragalactic sources with known redshifts². In total, 389 individual spectral points from 50 spectral measurements of 25 sources have been accumulated. A summary of the data is given in Table 1 including references. For a number of sources, the spectra have been measured at different times and with different instruments. Statistically independent measurements of identical sources are included in the sample. Objects without confirmed spectral determination of the redshift are excluded from the sample as well as individual measurements which at a later stage have been re-analysed or combined in a time-average measurement.

The observed spectral points $\varphi_i(E_i)$ for each source at redshift z are assigned an optical depth $\tau_i(E_i, z)$ using the minimal EBL model [22]. In Fig. 1, the locations of the measurements in the z, E -plane are indicated by an individual marker. Overlaid are the lines for constant optical depth $\tau = 1, 2, 3, 4$. For each observed spectral point, we can then readily calculate the spectral point corrected for the effect of absorption

$$\Phi_i = \exp(\tau_i)\varphi_i. \quad (2.1)$$

²nearby sources like M87 and Cen A have been excluded

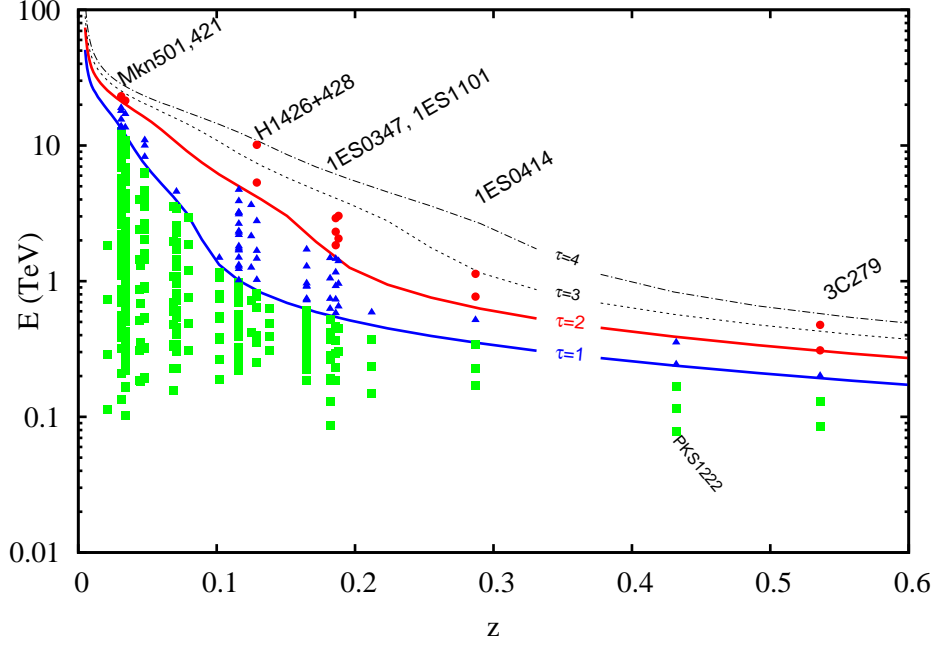


Figure 1. A summary of the spectral data used in this study: For each individual spectral measurement, the corresponding value of z and E are marked in this diagram. Overlaid are the iso-contours for $\tau = 1, 2, 3, 4$ calculated using the minimum EBL model.

id	Source	Redshift	Experiment	Energy Range (TeV)	Reference
1	3C66B	0.021	MAGIC	0.11 – 1.85	[25]
2	Mkn421	0.031	HEGRA	0.56 – 6.86	[26]
3	Mkn421	0.031	HEGRA	0.82 – 13.59	[27]
4	Mkn421	0.031	HEGRA	0.82 – 13.59	[27]
5	Mkn421	0.031	HESS	1.12 – 17.44	[28]
6	Mkn421	0.031	WHIPPLe	0.38 – 8.23	[29]
7	Mkn421	0.031	MAGIC	0.13 – 1.84	[30]
8	Mkn421	0.031	MAGIC	0.45 – 4.24	[31]
9	Mkn421	0.031	HESS	1.73 – 23.1	[32]
10	Mkn501	0.034	HEGRA	0.56 – 21.45	[33]
11	Mkn501	0.034	CAT	0.40 – 10.00	[34]
12	Mkn501	0.034	VERITAS	0.27 – 3.86	[35]
13	Mkn501	0.034	VERITAS	0.22 – 1.90	[36]
14	Mkn501	0.034	VERITAS	0.25 – 3.89	[37]
15	Mkn501	0.034	MAGIC	0.17 – 4.43	[37]
16	Mkn501	0.034	VERITAS	0.26 – 3.80	[35]
17	Mkn501	0.034	MAGIC	0.10 – 1.76	[38]
18	Mkn501	0.034	VERITAS	0.25 – 3.81	[37]
19	1ES2344+514	0.044	MAGIC	0.19 – 4.00	[39]
20	Mkn180	0.045	MAGIC	0.18 – 1.31	[40]

Continued on next page

Table1– continued from previous page

id	Source	Redshift	Experiment	Energy Range (TeV)	Reference
21	1ES1959+650	0.048	HEGRA	1.59 – 10.00	[41]
22	1ES1959+650	0.048	HEGRA	1.52 – 10.94	[41]
23	1ES1959+650	0.048	MAGIC	0.19 – 1.53	[42]
24	1ES1959+650	0.048	MAGIC	0.19 – 2.40	[43]
25	BLLacertae	0.069	MAGIC	0.16 – 0.70	[44]
26	PKS0548-322	0.069	HESS	0.34 – 3.52	[45]
27	PKS2005-489	0.071	HESS	0.23 – 2.27	[46]
28	PKS2005-489	0.071	HESS	0.34 – 4.57	[47]
29	RGBJ0152+017	0.080	HESS	0.31 – 2.95	[48]
30	W Comae	0.102	VERITAS	0.26 – 1.15	[49]
31	W Comae	0.102	VERITAS	0.19 – 1.49	[50]
32	PKS2155-304	0.116	HESS	0.23 – 2.28	[51]
33	PKS2155-304	0.116	HESS	0.23 – 3.11	[52]
34	PKS2155-304	0.116	HESS	0.22 – 4.72	[53]
35	PKS2155-304	0.116	HESS	0.25 – 3.20	[54]
36	RGBJ0710+591	0.125	VERITAS	0.42 – 3.65	[55]
37	H1426+428	0.129	HEGRA,CAT,WHIPPLE	0.25 – 10.12	[8]
38	1ES0806+524	0.138	MAGIC	0.31 – 0.63	[56]
39	1ES0229+200	0.140	HESS	0.60 – 11.45	[57]
40	H2356-309	0.165	HESS	0.22 – 0.91	[58]
41	H2356-309	0.165	HESS	0.23 – 1.71	[59]
42	H2356-309	0.165	HESS	0.18 – 0.92	[18]
43	1ES1218+304	0.182	MAGIC	0.09 – 0.63	[60]
44	1ES1218+304	0.182	VERITAS	0.19 – 1.48	[61]
45	1ES1101-232	0.186	HESS	0.18 – 2.92	[18]
46	1ES0347-121	0.188	HESS	0.30 – 3.03	[62]
47	1ES1011+496	0.212	MAGIC	0.15 – 0.59	[63]
48	1ES0414+009	0.287	HESS	0.17 – 1.13	[64]
49	PKS1222+21	0.432	MAGIC	0.08 – 0.35	[65]
50	3C279	0.536	MAGIC	0.08 – 0.48	[66]

Table 1: TeV blazar spectra used in this paper ordered by red-shift. The spectra which contain data-points with optical depth $\tau > 2$ are marked with bold-face.

2.2 Method to search for the anomaly

For each spectrum, the data points observed in the optically thin regime are identified by requiring $\tau < 1$. These data points are the basis to determine the parameters of a fitting function $f_{id}(E)$ to Φ_i . The fitting function describes the shape of the energy spectrum within the optically thin regime and therefore should be close to the intrinsic spectral shape. The fitting function is a power law of the form $f_{id}(E) = f_0(E/E_d)^{-\Gamma}$ with two free parameters for each source (id): the normalization f_0 and the photon index Γ . The best-fitting parameters are found with a χ^2 -minimization procedure. The decorrelation energy E_d is chosen such that the covariance matrix is diagonal. The p -value for the resulting value of χ^2 and degrees-of-freedom (dof) of the fit is calculated and used as a goodness-of-fit estimator. If the p -value

is smaller than 0.05, a more complex fitting function is chosen to be a log-log parabola $f_{\text{id}}(E) = f_0(E/E_d)^{-\Gamma+\beta\log(E/E_d)}$. The curved spectrum is used to fit the energy spectra of Mkn 421 ($id = 2, 3, 5, 7$), Mkn 501 ($id = 10, 11$), and PKS 2155-305 ($id = 34$) during high flux states satisfactorily. Any spectra which can not be described with $p > 0.05$ ($id = 7$) or have less than two spectral points with $\tau < 1$ ($id = 39$) are rejected from the sample. The final data sample consists of 389 spectral points with 305 optically thin measurements.

The data points with optical depth $\tau \geq 1$ are further split into a reference (base) sample $\mathcal{B} = \{\Phi_i | 1 \leq \tau_i < 2\}$ and the search sample $\mathcal{S} = \{\Phi_i | 2 \leq \tau_i\}$. The intervals chosen are guided by the expected effect of the coupling to an axion-like particle which leads to a boost of the observed flux at optical depth beyond approximately two [23].

For each flux point in \mathcal{B} and \mathcal{S} , we calculate a quantity which provides a measure on how the flux points scatter around the extrapolated expectation from the optically thin spectrum:

$$R(\Phi_i) = \frac{\Phi_i - f_{\text{id}}(E_i)}{\Phi_i + f_{\text{id}}(E_i)}. \quad (2.2)$$

So far, the estimated uncertainties (both statistical and systematic) on φ_i have been ignored. The systematic effects will be subject of discussion in the following subsection (3). The statistical uncertainties can not be included in the test, because the observed scatter of the measurements around the fit indicate that the error estimates are larger than the actual scatter. This follows from the consideration of the distribution of the normalized residuals

$$\chi_i := \frac{\Phi_i - f_{\text{id}}(E_i)}{\sigma(\Phi_i)}, \quad (2.3)$$

which does not follow a $N(\mu, \sigma)$ normal distribution with $\mu = 0$ and $\sigma = 1$ as expected. An unbinned likelihood fit of χ provides best-fit estimators for $\mu = 0.04 \pm 0.05$ and $\sigma = 0.78 \pm 0.03$ (errors quoted are estimated for 68 % confidence intervals). Interestingly, the distribution is barely compatible with a Gaussian (performing an Anderson-Darling test, the probability for a normal distribution is 1.7 %). As can be seen in Fig. 2, the distribution shows tails towards both negative as well as positive values indicating that the power law assumption is in slight tension with the actual spectra. Similar results for the width of the distribution of χ have been obtained for spectra of Galactic sources. It remains unclear why the true observational uncertainties are universally smaller than the estimated ones. In principle, the errors could be scaled by a factor 0.78 in order to match the errors with the observed scatter, but it appears difficult to draw firm conclusions on scaled errors. A close inspection of the residuals in different intervals of energy and optical depth (see Appendix B) indicates that the scatter of the residuals varies for the different samples considered, making it unreasonable to apply a global scaling of the estimated uncertainties. Instead, the test advocated here takes self-consistently the scatter of the data into account and does not rely on properly estimated errors.

2.3 Results of the test

The distribution of $R(\Phi_i \in \mathcal{B})$ with $N_1 = 63$ values is finally compared with the distribution of $R(\Phi_i \in \mathcal{S})$ ($N_2 = 13$) using the unbinned Kolmogorov-Smirnov (K-S) test on the empirical cumulative distribution function (CDF) (the individual spectra which contributed to the \mathcal{S} -sample are shown in Fig. 7). The K-S test does not rely on error estimates and is mainly sensitive to a relative shift of the two distributions while the presence of tails or a difference in the distribution widths does not strongly affect the test. For the maximum difference of the

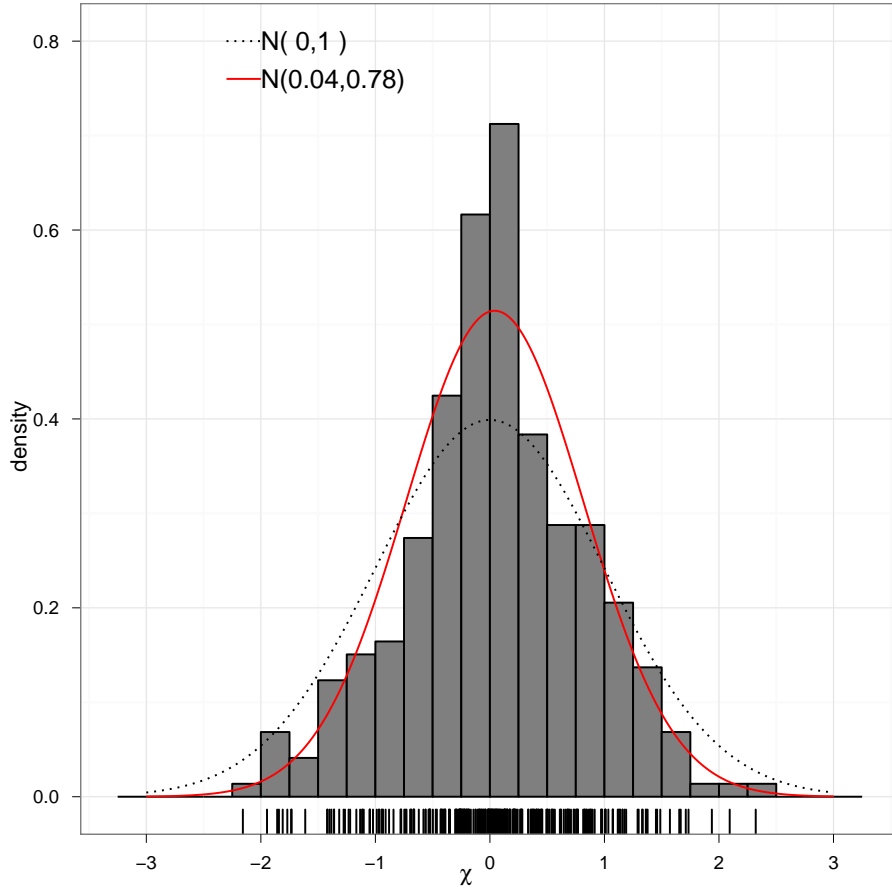


Figure 2. The distribution of the error-normalized scatter of individual values of Φ_i which enter the fit ($\tau < 1$): For comparison, a normal distribution $N(0,1)$ is overlaid (dashed line) together with the best fitting normal distribution with mean 0.04 ± 0.05 and width $\sigma = 0.78 \pm 0.03$.

two CDFs of $D = 0.703$, the resulting probability that the two distributions originate from the same parent distribution is $p(> D, N_1, N_2) = 1.7 \times 10^{-5}$ corresponding to a one-sided tail of a Gaussian at $S = 4.2 \sigma$ (see Fig. 3 for a graphical representation of the CDFs). The result indicates a shift of the distribution for the values in the \mathcal{S} -sample when comparing with the \mathcal{B} -sample. The two samples show also a quite different behaviour when considering the correlation of R and τ . For the sample \mathcal{B} , a Pearson's test on the correlation results in $cor(\mathcal{B}) = -0.09 \pm 0.12$ with a probability for the hypothesis of uncorrelated data $p(\mathcal{B}) = 0.46$. The search sample shows a moderate indication for a correlation: $cor(\mathcal{S}) = 0.35 \pm 0.25$ and $p(\mathcal{S}) = 0.23$. This behaviour is apparent when producing a scatter-plot of R versus τ as shown in Fig. 4. In addition to the K-S test applied to statistically independent samples of R -values, we have used in Appendix B the sample of residuals of a fit applied to all measurements. Consistent with the result of the K-S test, the average of the residuals for the sample $\chi_i(\mathcal{S})$ is significantly shifted away from zero ($\mu = 0.73 \pm 0.13$) which indicates a shift of 5.6σ . It should be noted, that this result is obtained with the additional assumption that the residuals are normal distributed. Given the reasonable p -values of the Anderson-Darling

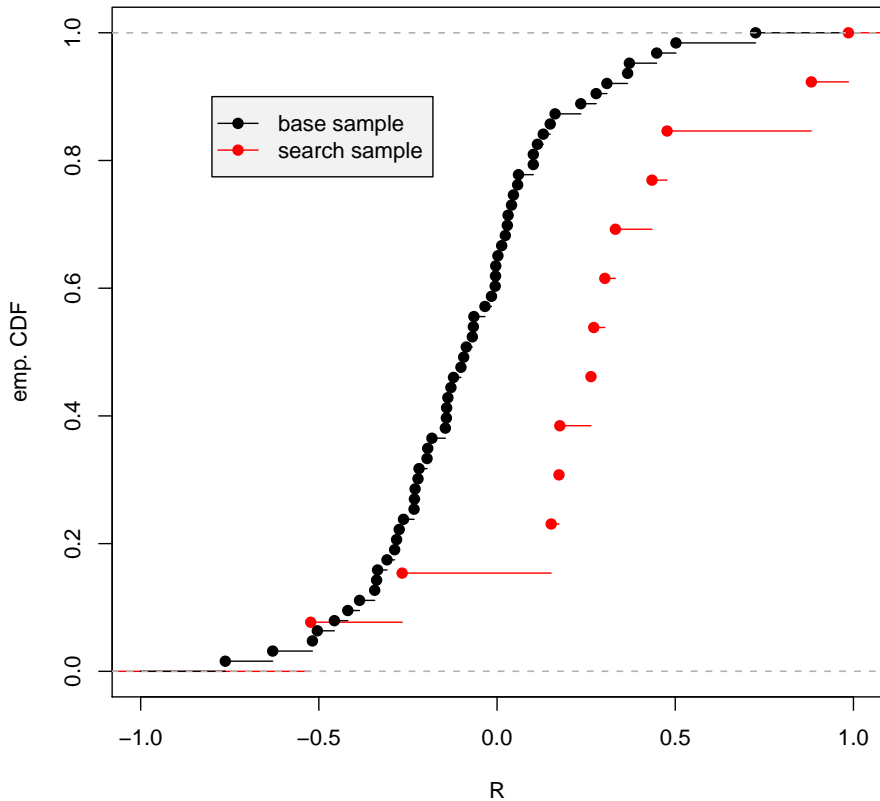


Figure 3. For the two samples (\mathcal{B} : base and \mathcal{S} : search) the empirical cumulative distribution functions (CDF) are compared. The two-sample Kolmogorov-Smirnov test statistics indicate that the probability for the two samples to be drawn from the same underlying distribution is 1.7×10^{-5} (corresponding to $S = 4.2 \sigma$).

test applied to the distribution of χ_i (see Appendix B for details), this assumption seems well justified.

3 Systematic effects

The result obtained in the previous section can be subject to systematic effects which are not related to the propagation of the photons. In the following, various systematic effects are considered.

3.1 Systematic effects related to the sources

The choice of blazars included in the sample is strongly biased by their detection at 100 GeV to TeV energies thus selecting preferentially objects with a sufficiently large luminosity. The seven sources with measurements extending to $\tau > 2$ contribute about equally to the overall excess. Removing each source spectrum and re-calculating the significance given in the

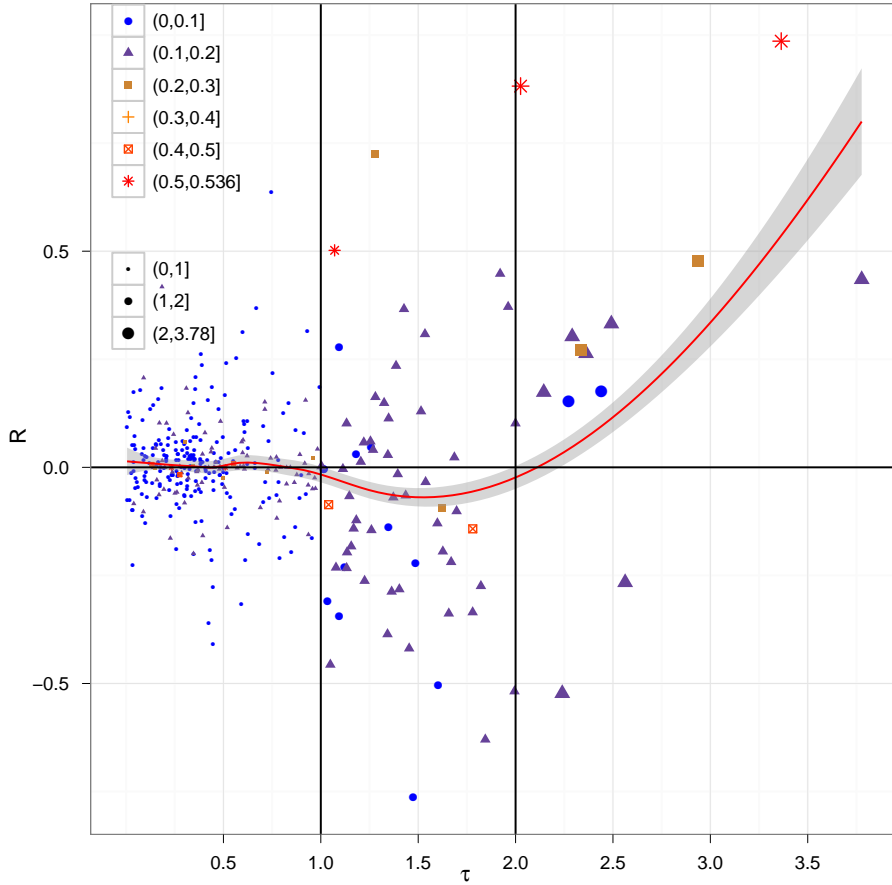


Figure 4. Scatter-plot of R vs τ . The color/shape of the markers indicate the redshift interval and the size of the marker is proportional to the optical depth. The solid line and grey band are derived from a non-parametric linear smoothing method (loess) and an estimate of the corresponding confidence interval (95 % c.l.) [67].

following list provides an estimate on the relevance of each source: Mkn 421 ($S(\overline{\text{Mkn 421}}) = 3.8 \sigma$), Mkn 501 ($S(\overline{\text{Mkn 501}}) = 3.7 \sigma$), H 1426+428 ($S(\overline{\text{H 1426 + 428}}) = 3.5 \sigma$), 1ES1101-232 ($S(\overline{\text{1ES1101 - 232}}) = 2.8 \sigma$), 1ES0347-121 ($S(\overline{\text{1ES0347 - 121}}) = 4.6 \sigma$), 1ES0414+009 ($S(\overline{\text{1ES0414 + 009}}) = 3.6 \sigma$), 3C279 ($S(\overline{\text{3C279}}) = 3.8 \sigma$). The result demonstrates that the different objects (6 high frequency peaked Blazars and 1 flat spectrum radio quasar) at widely different redshifts ($z = 0.031, 0.034, 0.129, 0.186, 0.188, 0.287$, and 0.536) contribute about equally to the overall significance. A systematic effect based upon the type of source or its distance is not evident. Note, the significance increases after excluding the spectrum of 1ES0347-121 from the overall test. This is a consequence of the extra-polation of the fit to the two points at small optical depth (see Fig. 7e). An unbiased or even complete catalogue of VHE-emitting blazars is at this point not available and will require an all-sky instrument with sufficient sensitivity (e.g. HAWC [68]). Instead, search strategies using narrow field of view instruments rely on external triggers indicating a high-state of an object or selection of bright objects from radio or X-ray catalogues or a mixture of both approaches. A successful detection is possible if the source is sufficiently bright in gamma-rays and if the observable

spectrum favors a detection. It is therefore conceivable, that redshift dependent selection effects favor e.g. the detection of blazars with softer spectra at large redshift. Generally, it is difficult to predict the selection bias without further knowledge on the relation between the spectral state and the luminosity of the source and the analysis carried out.

The test applied here does not depend on any prior assumption on the shape of the source spectrum and is therefore not sensitive to selection biases or even multiple-components in the high-energy part of the spectra as e.g. possibly present in Fermi-LAT spectra [69] and explained in the framework of time-dependent models for gamma-ray flares [70]. By construction, the test only probes the transition region from $\tau < 2$ to $\tau > 2$. Given that the energy at which this transition takes place varies in a non-linear way with redshift, it is very unlikely that any of the selection biases or spectral features present in the source could depend on redshift in the same way. The fact that widely different sources at different redshifts contribute to the observed anomaly strengthens this argument.

In Fig. 5, the scatter-plot of R vs $\log_{10}(E/\text{TeV})$ demonstrates that the source spectra behave rather similarly across the entire energy band covered by observations. The residuals analysed in Appendix B show a consistent behaviour. The notable deviations are measurements with optical depth $\tau > 2$. This indicates that the sources do not show any particular deviations from the assumed fitting function and its extrapolation across the entire energy range except the optically deep regime. In conclusion, a source intrinsic hardening of the energy spectrum is not excluded and may also be motivated in particularly tuned models [71]. However, there are no indications for spectral hardening in the gamma-ray spectra except for the spectra observed at optical depth $\tau > 2$ which rules out that this hardening is source-intrinsic.

3.2 Energy calibration

The energy scale of the ground based Cherenkov telescopes could be erroneous. Nominally, the experimental groups estimate the systematic uncertainty on the global energy scale to be $\approx \pm 15\%$ on a relative scale. In a recent study [72], the flux normalization of the Crab nebula between the different Cherenkov telescopes has been compared among each other in order to estimate systematic differences between the energy calibration of HESS, MAGIC, and HEGRA. Relative to the lowest energy calibration (HESS), the energy scale of MAGIC and HEGRA is shifted upwards by $(7 \pm 1)\%$ and $(8 \pm 1)\%$ respectively. Moreover, a cross calibration with the Fermi/LAT demonstrates a surprisingly small difference ($< 5\%$) of the energy calibration of air shower measurements with respect to the beam-calibrated pair telescope. Varying the energy calibration of all instruments between 5 and 10% downwards leads to a maximum reduction of resulting p -value to 4×10^{-4} (3.3σ). For the maximum admitted shift of the energy scale (-15%), the energy spectrum of 1ES0229+200 is included in the test leading to a smaller value of $p = 2.9 \times 10^{-4}$ (3.4σ). Nominally, this source is not included because only one data point with $\tau < 1$ is not sufficient to provide a power law fit. After shifting the energy scale downwards, this source is included compensating partially for the effect of the shift on other sources.

3.3 End-point of the energy spectra

The optically thick data points are naturally at the endpoint of the measured energy spectra. In this regime, the observed spectra suffer from the limited energy resolution leading to spill-over effects. In combination with a softening of the observed energy spectrum at high energies, the spill-over effect could lead to a systematic over-estimate of the true flux. In combination with the exponential factor multiplied to compensate the effect of absorption,

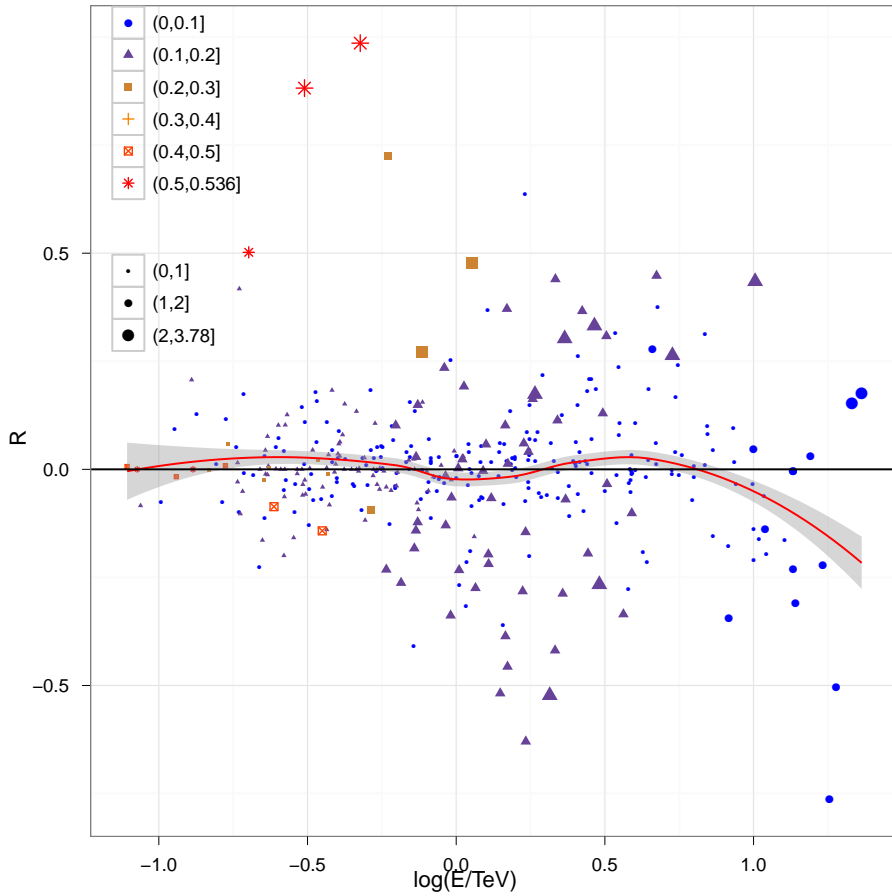


Figure 5. Scatter-plot of R vs $\log_{10}(E/\text{TeV})$. The color/shape of the markers indicate the redshift interval and the size of the marker is proportional to the optical depth. The solid line and grey band are derived from a quadratic smoothing method and an estimate of the corresponding confidence interval (68 % c.l.) [67].

this systematic effect could mimic the observed hardening. Furthermore, the endpoint of the energy spectrum is defined by the last significant detection. This leads to a unavoidable bias in the reconstructed flux which tends to be larger than the true flux. Without in-depth knowledge of the analysis methods, it is unrealistic to attempt to correct for these effects in a reliable way. As a simple and robust check on the bias on the analysis, we ignore the respective endpoint and shift the energy scale downwards by 15 %, maximizing the systematic influence on the test. The resulting significance is reduced, leading to $p = 4.8 \times 10^{-3}$ ($S = 2.6 \sigma$) which is certainly an upper limit to the true probability.

3.4 Mock data set

The test carried out could be biased intrinsically by the choice of the reference and search sample. The different scatter of the points in the two sample could lead to differences in the resulting distributions of R simply by the construction (e.g. extrapolation of the fit). As a mock sample, we choose energy spectra from Galactic sources with similar numbers of data points in a reference and search sample. Each spectrum is randomly assigned a redshift

to split the data points accordingly – however without applying a correction factor $\exp(\tau)$. After repeating the analysis, the resulting p -values are close to unity, demonstrating that the choice of reference and search sample does not lead automatically to differences in the resulting distribution.

4 Interpretation and discussion

After considering and rejecting the various possibilities to explain the observed effect by systematic uncertainties related to the observation and the source, it appears that the most likely explanation is related to the propagation of the photons. While a definite answer will certainly require a better characterization of the effect through either astrophysical observations or laboratory experiments or a combination of both, a number of possibilities can readily be excluded.

4.1 EBL

The level of EBL used for the test can be safely considered as a lower limit to the actual photon density in intergalactic space [22]. The anomaly appears at different energies (from 360 GeV to 22 TeV) which in turn relates to a broad range of wavelengths of the EBL between the optical to mid-IR. In order to eradicate the effect entirely, the EBL (maintaining the same shape) would have to be corrected downward by about 20 %. This would reduce the number of data points in the search sample to zero. Shifting the EBL downwards is, however, in contradiction with the observationally resolved part of the EBL: The scaled model falls below the lower limits derived from galaxy number counts in the UV / optical [73] and in the NIR [74] by more than one sigma of the measurement uncertainties. Another possibility would be to shift the EBL upwards and altering its shape. Three out of the seven sources in the sample are located at a redshift between $0.1 < z < 0.2$ and are measured up to a few TeV. Thus, the absorption corrected spectra of these sources are influenced most by changes of the EBL density between optical and NIR wavelengths. Increasing the EBL density at optical wavelengths leads to softening of the EBL corrected spectra and the signal significance is reduced. However, the effect observed for the other sources would be enhanced, partially compensating this effect.

4.2 Implications Pair-production anomaly

After excluding the sources, the EBL, and observational effects to explain all of the spectral signature, we consider the possibility of a pair-production anomaly (PPA). The effect could be explained if pair production in collisions of energetic photons (from 0.3 to 20 TeV) with low energy photons of the EBL is suppressed. A number of suggestions have been discussed in the literature which could lead to an effective pair-production anomaly.

- **Violation of Lorentz invariance:** Among the physically motivated possibilities, the violation of Lorentz invariance and its effect on the propagation of neutral particles has been considered in some detail. A high energy theory could in principle lead to a modification of the photon dispersion relation which would lead to an energy-dependent time-of-flight for photons as well as a shift of the threshold for pair production. In principle, the shift of threshold could lead to a suppression of pair production for higher energies. However, the observations indicate that the anomaly is seen at different energies depending upon the redshift of the source. This in turn is not expected within the

LIV scheme which predicts a fixed energy above which the optical depth is suppressed. In principle, in models of D-branes, different line-of-sights could be affected in different ways [75]. However, it would require a very unlikely finetuning of the model in order to explain the observed effect.

- **Axion-like particles:** A more likely scenario is the mixing of the photon with a spin-0 boson which would suppress the effect of pair production in the observed way. In the most general form, mixing during propagation in the intergalactic medium with a given domain size [16, 17] would have to be combined with mixing in the source [23] and the Galactic magnetic field [76]. Given the large range of possible combinations of parameters (domain size and product of magnetic field and coupling $g_{a\gamma}$) including stochastic variations along the different line of sights as well as an unknown shape of the true EBL, it is well beyond the scope of this paper and the data available to derive a reliable estimate of the most likely coupling and mass of the mixing partner of the photon. However, a qualitative estimate comparison has been done. The result is shown in Fig. 6 where the same data are shown as in Fig. 5. Overlaid is now a set of curves which provide an estimate on how much the transparency would change in the presence of a pseudo-scalar field which couples to photons with $g_{a\gamma} = 10^{-11}\text{GeV}^{-1}$ in the presence of an intergalactic magnetic field of 1 nG and domains of random orientation of the B -field and length of 5 Mpc. The chosen value for the field strength is not ruled out by observational bounds (see e.g. [77] for a compilation of available limits)³. The average transfer matrix has been calculated using the solution obtained in [16] using self-consistently the same lower limit EBL. As can be readily seen from the graph, the qualitative behaviour matches the observational data quite well.

5 Summary and conclusion

In the past years, the VHE spectroscopy of extragalactic objects has been considerably extended in energy and redshift covered. The currently available data have been collected and analysed for the first time in a comprehensive and consistent manner. The intrinsic spectral shapes have been recovered under the assumption of a minimum (guaranteed) absorption of VHE photons in pair production processes. A simple unbinned test has been introduced to search for the emergence of spectral features at the transition from optically thin to optically thick: the scatter of the spectral measurements around the extrapolation of a fit-function to the optically thin part of the spectrum ($\tau < 1$) is compared between well-defined samples covering ranges in optical depth of $1 \leq \tau < 2$ and $2 \leq \tau$. The two samples show differences at a significance level of $S = 4.2 \sigma$ ($S = 5.6 \sigma$ using the additional assumption of gaussianity of the residuals verified with the data) indicating that the observed absorption is smaller than the minimum absorption assumed. A number of systematic effects (e.g. shift of energy scale, flux bias at the end of the spectra) have been considered but found unlikely to provide the exclusive explanation for the observed effect. Source intrinsic features are unlikely to explain the upturn of the spectra at $\tau > 2$ unless an unnatural finetuning of the source with the optical depth at which it is observed exists. As a result of the study presented here, we conclude that the observations indicate the presence of a suppression of pair production

³Recently, observational evidence has been discussed that the intergalactic medium is efficiently heated through generation of plasma-instabilities by powerful blazars [78–81]. If this heating mechanism is at work, it would imply a model-dependent upper limit on the field strength of $\approx 10^{-12}$ G.

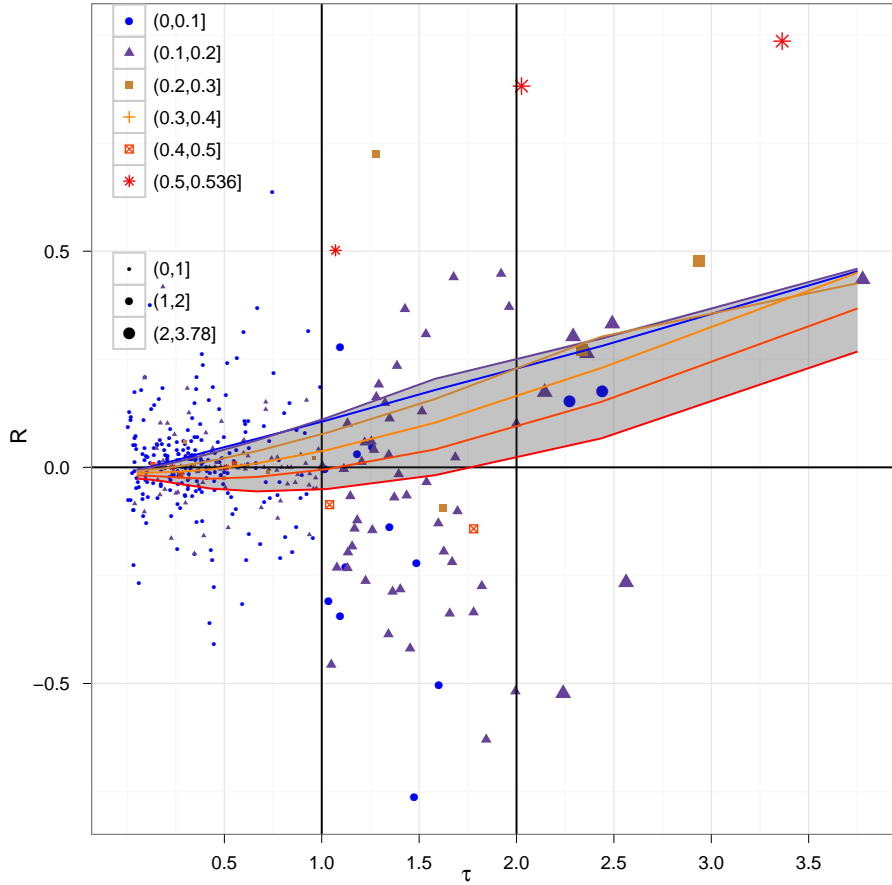


Figure 6. Overlaid on the same data as shown in Fig. 5 is a set of curves for different redshifts indicating the change of the transparency if a spin-0 axion-like particle would couple to photons. The parameters chosen were $g_{a\gamma} = 10^{-11} \text{ GeV}^{-1}$, $l = 5 \text{ Mpc}$, $B = 1 \text{ nG}$.

during the propagation of VHE photons which is coined “pair-production anomaly” (PPA). The data do not allow to constrain the properties of the PPA but a plausible explanation is provided by coupling photons to a pseudo-scalar (axion-like particles) via intergalactic magnetic fields.

Acknowledgments

We thank Tanja Kneiske, Martin Raue, Andrei Lobanov, Javier Redondo, Alessandro Mirizzi, Andreas Ringwald, and Marco Roncadelli for valuable input and discussions on this theme. We thank the anonymous referee for constructive comments. MM acknowledges the support of the Hamburg cluster of excellence *Connecting Particles with the Cosmos*. DH acknowledges the support of the collaborative research center SFB 676 *Particles, Strings, and the Early Universe*. This research has made use of NASA’s Astrophysics Data System.

References

- [1] R. J. Gould and G. P. Schröder, *Pair Production in Photon-Photon Collisions*, *Phys.Rev.* **155** (Mar., 1967) 1404–1407.
- [2] R. J. Protheroe, *Effect of electron-photon cascading on the observed energy spectra of extragalactic sources of ultra-high-energy gamma-rays*, *MNRAS* **221** (Aug., 1986) 769–788.
- [3] M. Ahlers and J. Salvado, *Cosmogenic gamma rays and the composition of cosmic rays*, *Phys.Rev.D* **84** (Oct., 2011) 085019, [[arXiv:1105.5113](#)].
- [4] K. Murase, C. D. Dermer, H. Takami, and G. Migliori, *Blazars as Ultra-High-Energy Cosmic-Ray Sources: Implications for TeV Gamma-Ray Observations*, *ArXiv e-prints* (July, 2011) [[arXiv:1107.5576](#)].
- [5] E. Armengaud, G. Sigl, and F. Miniati, *Secondary gamma rays from ultrahigh energy cosmic rays produced in magnetized environments*, *Phys.Rev.D* **73** (Apr., 2006) 083008.
- [6] W. Essey and A. Kusenko, *A new interpretation of the gamma-ray observations of distant active galactic nuclei*, *Astroparticle Physics* **33** (Mar., 2010) 81–85, [[arXiv:0905.1162](#)].
- [7] W. Essey, O. Kalashev, A. Kusenko, and J. F. Beacom, *Role of Line-of-sight Cosmic-ray Interactions in Forming the Spectra of Distant Blazars in TeV Gamma Rays and High-energy Neutrinos*, *Astrophys.J.* **731** (Apr., 2011) 51, [[arXiv:1011.6340](#)].
- [8] F. Aharonian and others (HEGRA coll.), *Observations of H1426+428 with HEGRA. Observations in 2002 and reanalysis of 1999–2000 data*, *Astron.Astrophys* **403** (May, 2003) 523–528, [[astro-ph/0301437](#)].
- [9] Wystan Benbow for the VERITAS Collaboration, *Highlights of the VERITAS Blazar Observation Program*, *ArXiv e-prints* (Sept., 2011) [[arXiv:1110.0038](#)].
- [10] A. Imran, *Analysis of variable VHE gamma-ray emission from the hard spectrum blazar 1ES 1218+304*. PhD thesis, Iowa State University, 2010.
- [11] S. Coleman and S. L. Glashow, *High-energy tests of Lorentz invariance*, *Phys.Rev.D* **59** (June, 1999) 116008–+, [[hep-ph/98](#)].
- [12] U. Jacob and T. Piran, *Inspecting absorption in the spectra of extra-galactic gamma-ray sources for insight into Lorentz invariance violation*, *Phys.Rev.D* **78** (Dec., 2008) 124010–+, [[arXiv:0810.1318](#)].
- [13] S. A. Abel, M. D. Goodsell, J. Jaeckel, V. V. Khoze, and A. Ringwald, *Kinetic mixing of the photon with hidden $U(1)$ s in string phenomenology*, *Journal of High Energy Physics* **7** (July, 2008) 124–+, [[arXiv:0803.1449](#)].
- [14] C. Csáki, N. Kaloper, M. Peloso, and J. Terning, *Super-GZK photons from photon axion mixing*, *JCAP* **5** (May, 2003) 5–+, [[hep-ph/03](#)].
- [15] A. de Angelis, M. Roncadelli, and O. Mansutti, *Evidence for a new light spin-zero boson from cosmological gamma-ray propagation?*, *Phys.Rev.D* **76** (Dec., 2007) 121301–+, [[arXiv:0707.4312](#)].
- [16] A. Mirizzi and D. Montanino, *Stochastic conversions of TeV photons into axion-like particles in extragalactic magnetic fields*, *JCAP* **12** (Dec., 2009) 4–+, [[arXiv:0911.0015](#)].
- [17] A. De Angelis, G. Galanti, and M. Roncadelli, *Relevance of axion-like particles for very-high-energy astrophysics*, *ArXiv e-prints* (June, 2011) [[arXiv:1106.1132](#)].
- [18] Aharonian, F. and others (H.E.S.S. coll.), *A Low level of extragalactic background light as revealed by gamma-rays from blazars*, *Nature* **440** (2006) 1018–1021, [[astro-ph/0508073](#)].
- [19] E. Dwek and F. Krennrich, *Simultaneous Constraints on the Spectrum of the Extragalactic Background Light and the Intrinsic TeV Spectra of Markarian 421, Markarian 501, and*

- H1426+428*, *Astrophys.J.* **618** (Jan., 2005) 657–674, [[astro-ph/](#)].
- [20] D. Mazin and M. Raue, *New limits on the density of the extragalactic background light in the optical to the far infrared from the spectra of all known TeV blazars*, *Astron.Astrop.* **471** (Aug., 2007) 439–452, [[astro-ph/](#)].
- [21] M. R. Orr, F. Krennrich, and E. Dwek, *Strong New Constraints on the Extragalactic Background Light in the Near- to Mid-infrared*, *Astrophys.J.* **733** (June, 2011) 77–+, [[arXiv:1101.3498](#)].
- [22] T. M. Kneiske and H. Dole, *A lower-limit flux for the extragalactic background light*, *Astron.Astrophys.* **515** (June, 2010) A19+, [[arXiv:1001.2132](#)].
- [23] M. A. Sánchez-Conde, D. Paneque, E. Bloom, F. Prada, and A. Domínguez, *Hints of the existence of axionlike particles from the gamma-ray spectra of cosmological sources*, *Phys.Rev.D* **79** (June, 2009) 123511–+, [[arXiv:0905.3270](#)].
- [24] A. Domínguez, M. A. Sánchez-Conde, and F. Prada, *Axion-like particle imprint in cosmological very-high-energy sources*, *JCAP* **11** (Nov., 2011) 20, [[arXiv:1106.1860](#)].
- [25] Aliu, E. and others (MAGIC coll.), *Discovery of a very high energy gamma-ray signal from the 3c 66a/b region*, *Astrophys. J.* **692** (2009) L29–L33, [[arXiv:0810.4712](#)].
- [26] Aharonian, F. and others (HEGRA coll.), *Observations of mkn 421 during 1997 and 1998 in the energy range above 500 gev with the hegra stereoscopic cherenkov telescope system*, *Astron.Astrophys.* **350** (1999) 757–764, [[9905032](#)].
- [27] Aharonian, F. and others (HEGRA coll.), *Variations of the TeV energy spectrum at different flux levels of Mkn 421 observed with the HEGRA system of Cherenkov telescopes*, *Astron.Astrophys.* **393** (2002) 89–100, [[astro-ph/0205499](#)].
- [28] F. Aharonian and others (H.E.S.S. coll.), *Observations of Mkn 421 in 2004 with HESS at large zenith angles*, *Astron.Astrophys.* **437** (July, 2005) 95–99, [[astro-ph/0506319](#)].
- [29] F. Krennrich, I. Bond, S. Bradbury, J. Buckley, D. Carter-Lewis, *et. al.*, *Discovery of spectral variability of Markarian 421 at TeV energies*, *Astrophys.J.* **575** (2002) L9–L14, [[astro-ph/0207184](#)].
- [30] Albert, J. and others (MAGIC coll.), *Observations of markarian 421 with the magic telescope*, *Astrophys. J.* **663** (2007) 125–138, [[0603378](#)].
- [31] Aleksić, J. and others (MAGIC coll.), *Magic tev gamma-ray observations of markarian 421 during multiwavelength campaigns in 2006*, *Astron.Astrophys.* **519** (2010) id. A32, [[arXiv:1001.1291](#)].
- [32] M. Tluczykont, *H.E.S.S. Observations of strong flaring activity of Mrk421 in February 2010*, *ArXiv e-prints* (June, 2011) [[arXiv:1106.1035](#)].
- [33] F. A. Aharonian and others (HEGRA coll.), *The time averaged TeV energy spectrum of MKN 501 of the extraordinary 1997 outburst as measured with the stereoscopic Cherenkov telescope system of HEGRA*, *Astron.Astrophys.* **349** (Sept., 1999) 11–28, [[astro-ph/](#)].
- [34] Djannati-Ataï, A. and Piron, F. and Barrau, A. and Iacoucci, L. and Punch, M. and others, *Very high-energy gamma-ray spectral properties of Mrk 501 from cat Cherenkov telescope observations in 1997*, *Astron.Astrophys.* **350** (1999) 17–24, [[astro-ph/9906060](#)].
- [35] D. Huang, A. Konopelko, and others for the VERITAS collaboration, *VERITAS Observations of Mkn 501 in 2009*, *ArXiv e-prints* (Dec., 2009) [[arXiv:0912.3772](#)].
- [36] D. Gall and others for the VERITAS Collaboration, *Multi-wavelength Observations of Markarian 501*, *ArXiv e-prints* (Dec., 2009) [[arXiv:0912.4728](#)].
- [37] A. A. Abdo *et. al.*, *Insights into the High-energy γ -ray Emission of Markarian 501 from Extensive Multifrequency Observations in the Fermi Era*, *Astrophys.J.* **727** (Feb., 2011) id 129,

- [arXiv:1011.5260].
- [38] H. Anderhub *et al.*, *Simultaneous Multiwavelength Observation of Mkn 501 in a Low State in 2006*, *Astrophys.J.* **705** (Nov., 2009) 1624–1631, [arXiv:0910.2093].
- [39] J. Albert and others (MAGIC coll.), *Observation of Very High Energy γ -Rays from the AGN 1ES 2344+514 in a Low Emission State with the MAGIC Telescope*, *Astrophys.J.* **662** (June, 2007) 892–899, [astro-ph/].
- [40] J. Albert and others (MAGIC coll.), *Discovery of Very High Energy γ -Rays from Markarian 180 Triggered by an Optical Outburst*, *Astrophys.J.* **648** (Sept., 2006) L105–L108, [astro-ph/0606630].
- [41] F. Aharonian and others (HEGRA coll.), *Detection of TeV gamma-rays from the BL Lac 1ES 1959+650 in its low states and during a major outburst in 2002*, *Astron.Astrophys.* **406** (July, 2003) L9–L13.
- [42] J. Albert and others (MAGIC coll.), *Observation of Very High Energy Gamma-Ray Emission from the Active Galactic Nucleus 1ES 1959+650 Using the MAGIC Telescope*, *Astrophys.J.* **639** (Mar., 2006) 761–765, [0508543].
- [43] G. Tagliaferri *et al.*, *Simultaneous Multiwavelength Observations of the Blazar 1ES 1959+650 at a Low TeV Flux*, *Astrophys.J.* **679** (June, 2008) 1029–1039, [arXiv:0801.4029].
- [44] J. Albert and others (MAGIC coll.), *Discovery of Very High Energy γ -Ray Emission from the Low-Frequency-peaked BL Lacertae Object BL Lacertae*, *Astrophys.J.* **666** (Sept., 2007) L17–L20, [astro-ph/0703084].
- [45] F. Aharonian and others (H.E.S.S. coll.), *Discovery of VHE gamma-rays from the BL Lac object PKS 0548-322*, *ArXiv e-prints* (June, 2010) [arXiv:1006.5289].
- [46] F. Aharonian and others (H.E.S.S. coll.), *Discovery of VHE gamma rays from PKS 2005-489*, *Astron.Astrophys.* **436** (June, 2005) L17–L20, [astro-ph/0504520].
- [47] F. Acero and others (H.E.S.S. coll.), *PKS 2005-489 at VHE: four years of monitoring with HESS and simultaneous multi-wavelength observations*, *Astron.Astrophys.* **511** (Feb., 2010) id A52, [arXiv:0911.2709].
- [48] F. Aharonian and others (H.E.S.S. coll.), *Discovery of VHE γ -rays from the high-frequency-peaked BL Lacertae object RGB J0152+017*, *Astron.Astrophys.* **481** (Apr., 2008) L103–L107, [arXiv:0802.4021].
- [49] V. A. Acciari and others (VERITAS coll.), *VERITAS Discovery of >200 GeV Gamma-Ray Emission from the Intermediate-Frequency-Peaked BL Lacertae Object W Comae*, *Astrophys.J.* **684** (Sept., 2008) L73–L77, [arXiv:0808.0889].
- [50] V. A. Acciari and others (VERITAS coll.), *Multiwavelength Observations of a TeV-Flare from W Comae*, *Astrophys.J.* **707** (Dec., 2009) 612–620.
- [51] Aharonian, F. and others (H.E.S.S. coll.), *H.E.S.S. observations of PKS 2155-304*, *Astron.Astrophys.* **430** (2005) 865–875, [astro-ph/0411582].
- [52] F. Aharonian and others (H.E.S.S. coll.), *Multi-wavelength observations of PKS 2155-304 with HESS*, *Astron.Astrophys.* **442** (Nov., 2005) 895–907, [astro-ph/0506593].
- [53] Aharonian, F. and others (H.E.S.S. coll.), *An Exceptional Very High Energy Gamma-Ray Flare of PKS 2155-304*, *Astrophys.J.* **664** (2007) L71–L78, [arXiv:0706.0797].
- [54] F. Aharonian and others (H.E.S.S. coll.), *Simultaneous Observations of PKS 2155-304 with HESS, Fermi, RXTE, and Atom: Spectral Energy Distributions and Variability in a Low State*, *Astrophys.J.* **696** (May, 2009) L150–L155, [arXiv:0903.2924].
- [55] V. A. Acciari, E. Aliu, T. Arlen, T. Aune, M. Bautista, and et al., *The Discovery of γ -Ray Emission from the Blazar RGB J0710+591*, *Astrophys.J.* **715** (May, 2010) L49–L55,

- [arXiv:1005.0041].
- [56] V. Acciari *et. al.*, *Discovery of Very High Energy Gamma-ray Radiation from the BL Lac 1ES 0806+524*, *Astrophys.J.* **690** (Jan., 2009) L126–L129, [arXiv:0812.0978].
- [57] F. Aharonian and others (H.E.S.S. coll.), *New constraints on the mid-IR EBL from the HESS discovery of VHE γ -rays from 1ES 0229+200*, *Astron.Astrophys.* **475** (Nov., 2007) L9–L13, [arXiv:0709.4584].
- [58] F. Aharonian and others (H.E.S.S. coll.), *Discovery of very high energy γ -ray emission from the BL Lacertae object H 2356-309 with the HESS Cherenkov telescopes*, *Astron.Astrophys.* **455** (Aug., 2006) 461–466, [astro-ph/0607569].
- [59] A. Abramowski and others (HESS Collaboration), *Multi-wavelength observations of H 2356-309*, *Astron.Astrophys.* **516** (June, 2010) A56+, [arXiv:1004.2089].
- [60] J. Albert and others (MAGIC coll.), *Discovery of Very High Energy Gamma Rays from 1ES 1218+30.4*, *Astrophys.J.* **642** (May, 2006) L119–L122, [astro-ph/0603529].
- [61] V. A. Acciari *et. al.*, *VERITAS Observations of the BL Lac Object 1ES 1218+30.4*, *Astrophys.J.* **695** (Apr., 2009) 1370–1375, [arXiv:0901.4561].
- [62] F. Aharonian and others (H.E.S.S. coll.), *Discovery of VHE γ -rays from the distant BL Lacertae 1ES 0347-121*, *Astron.Astrophys.* **473** (Oct., 2007) L25–L28, [arXiv:0708.3021].
- [63] J. Albert and others (MAGIC coll.), *Discovery of Very High Energy γ -Rays from 1ES 1011+496 at $z = 0.212$* , *Astrophys.J.* **667** (Sept., 2007) L21–L24, [arXiv:0706.4435].
- [64] A. Abramowski and others (HESS Collaboration), *Discovery of hard-spectrum γ -ray emission from the BL Lac object 1ES 0414+009*, *ArXiv e-prints* (Jan., 2012) [arXiv:1201.2044].
- [65] J. Aleksić *et. al.*, *MAGIC discovery of VHE Emission from the FSRQ PKS 1222+21*, *Astrophys.J.* **730** (Mar., 2011) L8, [arXiv:1101.4645].
- [66] Albert, J. and others (MAGIC coll.), *Very-High-Energy Gamma Rays from a Distant Quasar: How Transparent Is the Universe?*, *Science* **320** (2008) 1752, [arXiv:0807.2822].
- [67] W. Cleveland, E. Grosse, and M. J. Shyu, *Local Regression Models*, pp. 309–376. Chapman and Hall, New York, 1992.
- [68] HAWC collaboration, *On the sensitivity of the HAWC observatory to gamma-ray bursts*, *ArXiv e-prints* (Aug., 2011) [arXiv:1108.6034].
- [69] A. A. Abdo, M. Ackermann, I. Agudo, M. Ajello, H. D. Aller, and et al., *The Spectral Energy Distribution of Fermi Bright Blazars*, *Astrophys.J* **716** (June, 2010) 30–70, [arXiv:0912.2040].
- [70] E. Lefa, F. M. Rieger, and F. Aharonian, *Formation of Very Hard Gamma-Ray Spectra of Blazars in Leptonic Models*, *Astrophys.J.* **740** (Oct., 2011) 64, [arXiv:1106.4201].
- [71] E. Lefa, F. A. Aharonian, and F. M. Rieger, *“Leading Blob” Model in a Stochastic Acceleration Scenario: The Case of the 2009 Flare of Mkn 501*, *Astrophys.J.* **743** (Dec., 2011) L19, [arXiv:1108.4568].
- [72] M. Meyer, D. Horns, and H.-S. Zechlin, *The Crab Nebula as a standard candle in very high-energy astrophysics*, *Astron.Astrophys.* **523** (Nov., 2010) A2+, [arXiv:1008.4524].
- [73] P. Madau and L. Pozzetti, *Deep galaxy counts, extragalactic background light and the stellar baryon budget*, *MNRAS* **312** (Feb., 2000) L9–L15, [astro-ph/].
- [74] G. G. Fazio, M. L. N. Ashby, P. Barmby, J. L. Hora, J.-S. Huang, M. A. Pahre, Z. Wang, S. P. Willner, R. G. Arendt, S. H. Moseley, M. Brodwin, P. Eisenhardt, D. Stern, E. V. Tollestrup, and E. L. Wright, *Number Counts at $3 \mu\text{m} < \lambda < 10 \mu\text{m}$ from the Spitzer Space Telescope*, *Astrophys.J.Suppl.* **154** (Sept., 2004) 39–43, [astro-ph/].

- [75] J. Ellis, N. E. Mavromatos, and D. V. Nanopoulos, *Comments on ultra-high-energy photons and D-foam models*, *Physics Letters B* **694** (Oct., 2010) 61–64, [[arXiv:1004.4167](#)].
- [76] M. Simet, D. Hooper, and P. D. Serpico, *Milky Way as a kiloparsec-scale axionscope*, *Phys.Rev.D* **77** (Mar., 2008) 063001–+, [[arXiv:0712.2825](#)].
- [77] A. Neronov and D. V. Semikoz, *Sensitivity of γ -ray telescopes for detection of magnetic fields in the intergalactic medium*, *Phys.Rev.D* **80** (Dec., 2009) 123012, [[arXiv:0910.1920](#)].
- [78] A. E. Broderick, P. Chang, and C. Pfrommer, *The Cosmological Impact of Luminous TeV Blazars I: Implications of Plasma Instabilities for the Intergalactic Magnetic Field and Extragalactic Gamma-Ray Background*, *ArXiv e-prints* (June, 2011) [[arXiv:1106.5494](#)].
- [79] C. Pfrommer, P. Chang, and A. E. Broderick, *The Cosmological Impact of Luminous TeV Blazars III: Implications for Galaxy Clusters and the Formation of Dwarf Galaxies*, *ArXiv e-prints* (June, 2011) [[arXiv:1106.5505](#)].
- [80] P. Chang, A. E. Broderick, and C. Pfrommer, *The Cosmological Impact of Luminous TeV Blazars II: Rewriting the Thermal History of the Intergalactic Medium*, *ArXiv e-prints* (June, 2011) [[arXiv:1106.5504](#)].
- [81] E. Puchwein, C. Pfrommer, V. Springel, A. E. Broderick, and P. Chang, *The Lyman-alpha forest in a blazar-heated Universe*, *ArXiv e-prints* (July, 2011) [[arXiv:1107.3837](#)].

A Energy spectra

The figures [7a-7g](#) show the energy spectra of the seven sources with spectral measurements in the optically thin as well as in the optically thick regime.

B Distribution of averaged residuals

The test introduced in Section 2 is based upon the null hypothesis that the independent samples of $R(\Phi_i \in \mathcal{B})$ and $R(\Phi_i \in \mathcal{S})$ stem from the same underlying unknown distribution. The best-fit parameters were derived by a χ^2 -minimization to the optically thin data-points. In the following, this assumption is tested by investigating the behaviour of the residuals χ_i as defined in Eqn. 2.2 after fitting f_{id} to the entire spectrum. In Fig. [8a](#), the normalised histogram of residuals is shown in three exclusive intervals of energy together with a normal distribution with μ and σ chosen to match the mean and \sqrt{var} of the samples chosen. The samples are consistent with normal distributions: Anderson-Darling tests estimates probabilities of 0.77, 0.68, and 0.43 for the three samples to be normal distributed. The average values of the residuals are all within one standard deviation of the mean consistent with zero. The scatter of the samples is distinctly different from the expected value, indicating that the experimental errors are over-estimated.

When taking the same residuals and considering the samples split according to the optical depth (using the same ranges as for the previous tests), again fairly normal distributed residuals are found (Anderson-Darling test: 0.07, 0.44, and 0.12, the width is again too narrow). The average residuals in the first two bins of τ are consistent with zero. For the last bin, the average residual of $\mu = 0.73 \pm 0.13$ is significantly different from zero ($S = 5.6 \sigma$), confirming the result obtained using the Kolmogorov-Smirnov test on the samples of R . The average values are compared for the different samples in Figs. [9a-9b](#).

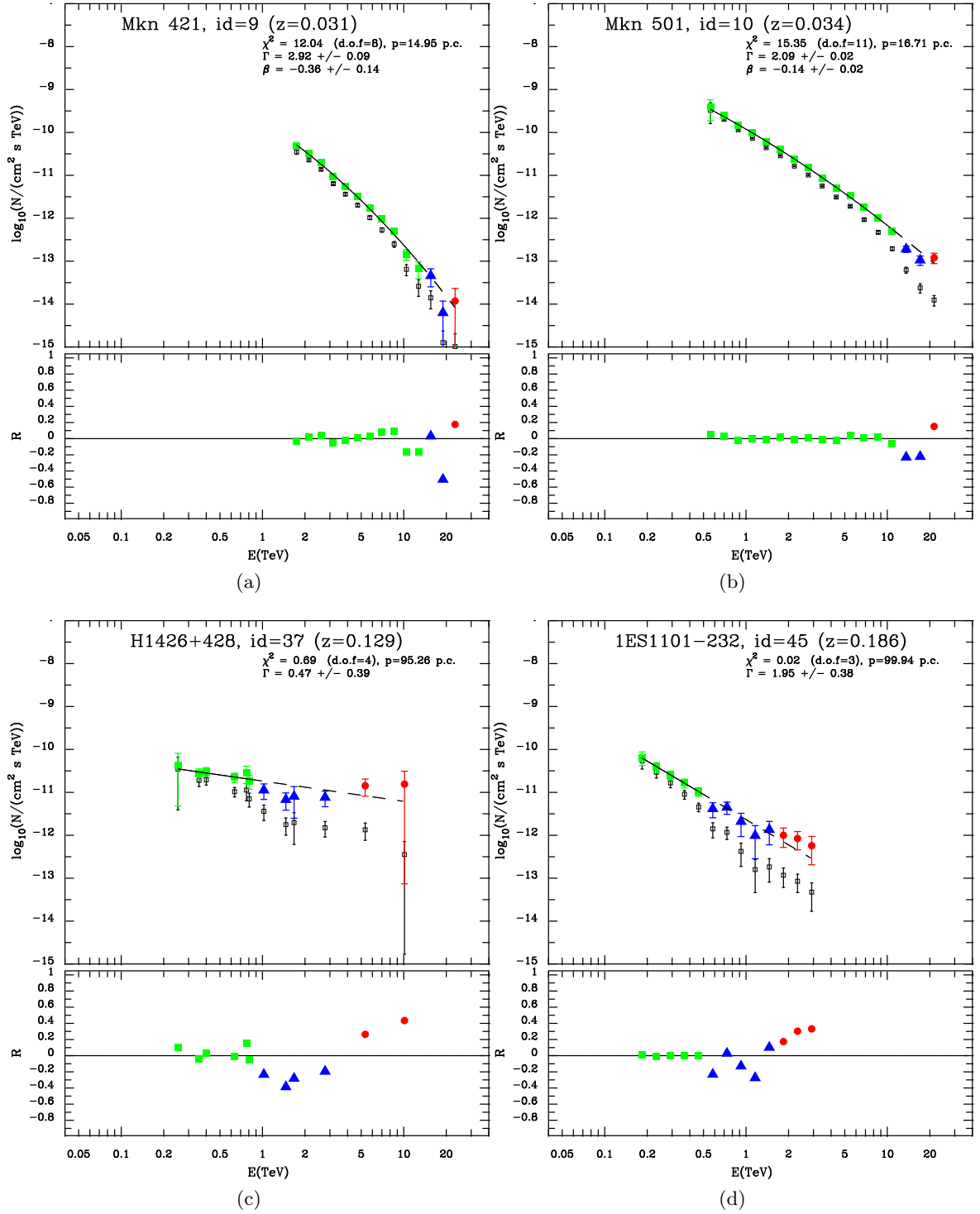


Figure 7. VHE energy spectra of AGN: The black open squares indicate the measured differential spectra while the coloured solid markers are the measurements corrected for absorption (squares/green: $\tau < 1$, triangles/blue: $1 \leq \tau < 2$, bullets/red: $2 \leq \tau$).

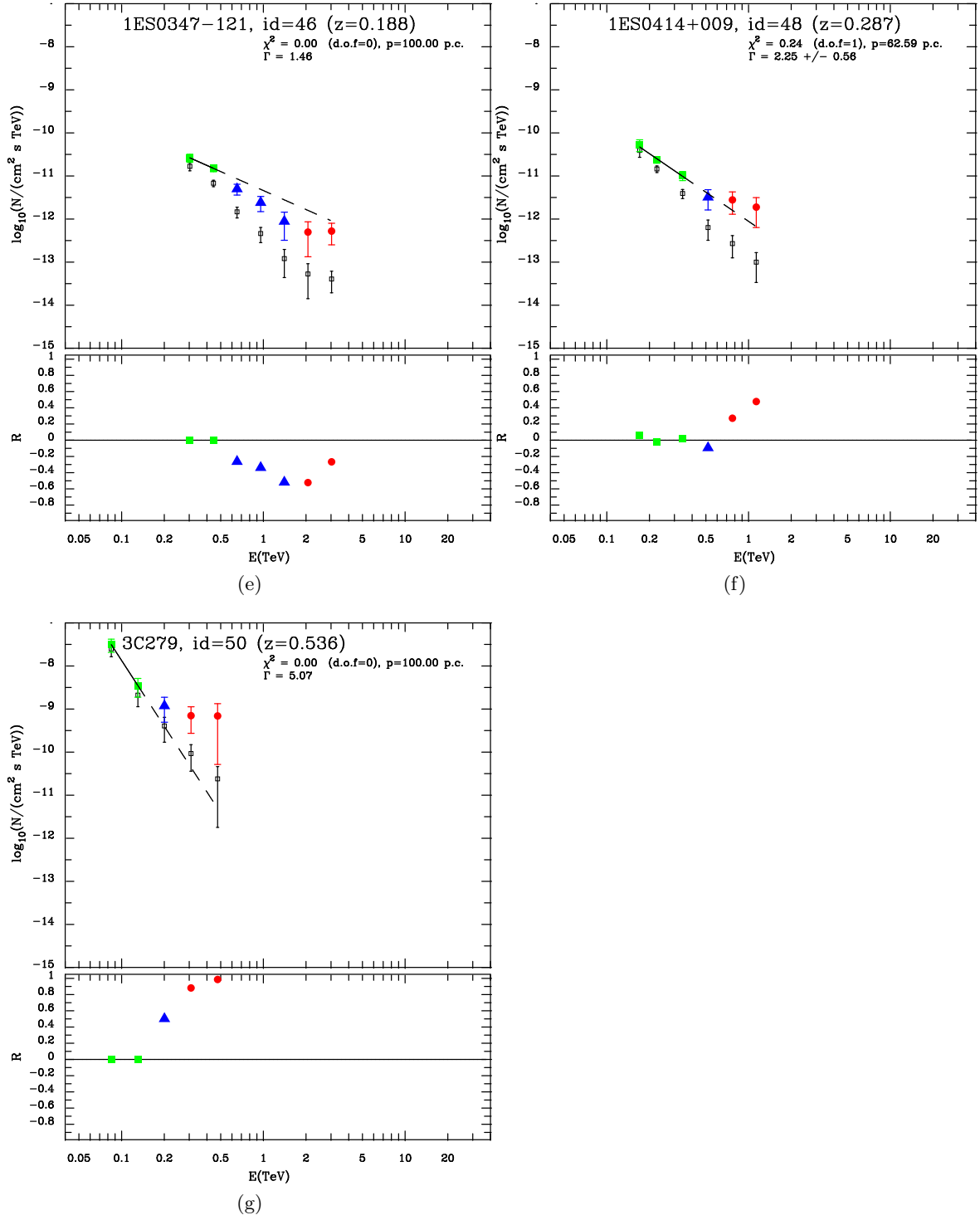


Figure 7. Energy spectra of Blazars: The black open squares indicate the measured differential spectra while the coloured solid markers are the measurements corrected for absorption (squares/green: $\tau < 1$, triangles/blue: $1 \leq \tau < 2$, bullets/red: $2 \leq \tau$).

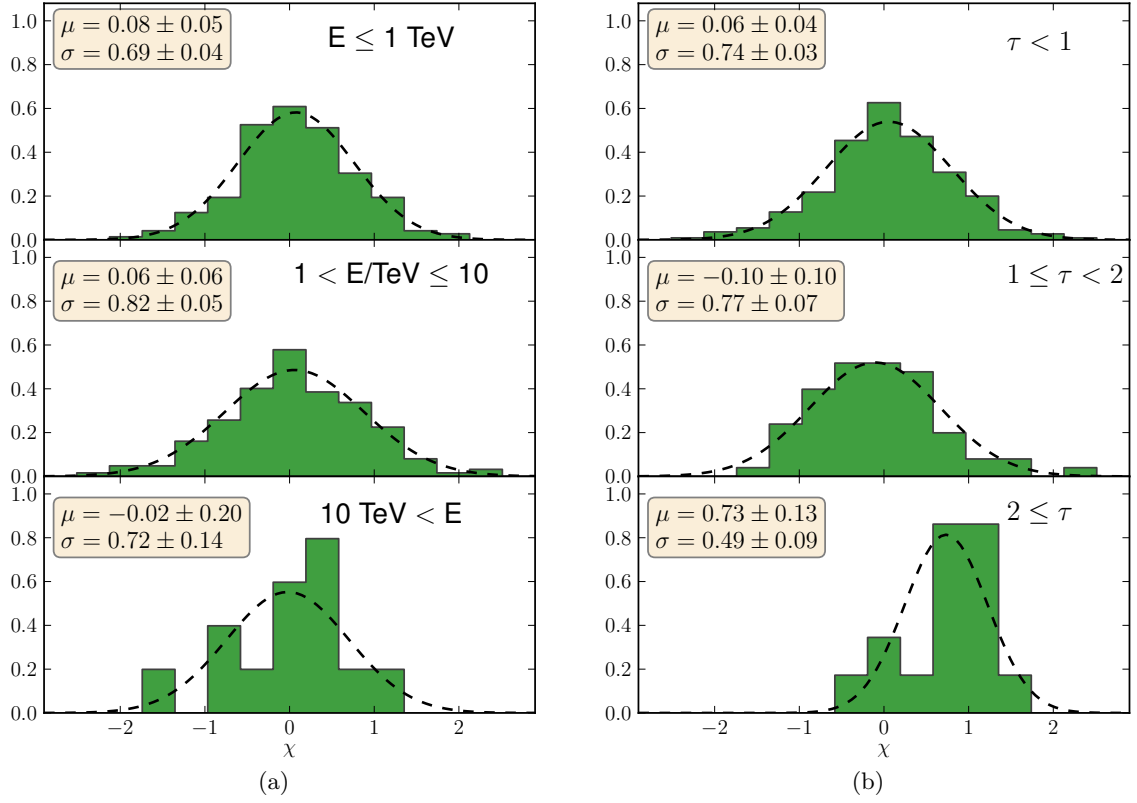


Figure 8. Normalised histograms of residuals in three intervals of energy (a) and optical depth (b), overlaid with dashed lines are the best-fit normal distributions.

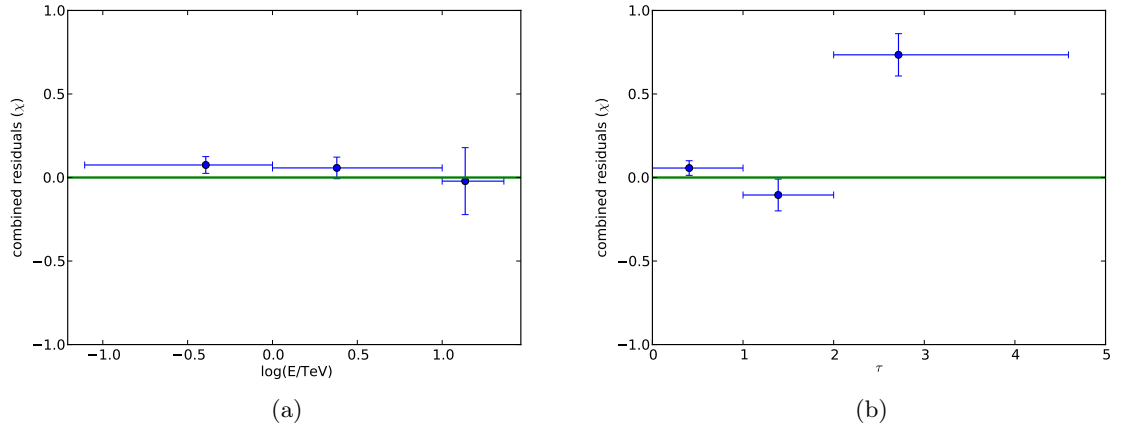


Figure 9. Average residuals (μ) and errors for three intervals of energy (a) and optical depth (b), the horizontal error bars indicate the range of values included in each bin, the vertical error bars show the 1σ uncertainty on μ .